Journal of Colloid and Interface Science 394 (2013) 69–77

Contents lists available at SciVerse ScienceDirect

Journal of Colloid and Interface Science

www.elsevier.com/locate/jcis

Microwave-assisted synthesis and photocatalytic properties of flower-like Bi_2WO_6 and Bi_2O_3–Bi_2WO_6 composite

Zhao-Qian Li [a], Xue-Tai Chen [a,*], Zi-Ling Xue [b]

[a] State Key Laboratory of Coordination Chemistry, Nanjing National Laboratory of Microstructures, School of Chemistry and Chemical Engineering, Nanjing University, Nanjing 210093, PR China
[b] Department of Chemistry, The University of Tennessee, Knoxville, TN 37996-1600, USA

ARTICLE INFO

Article history:
Received 23 July 2012
Accepted 3 December 2012
Available online 22 December 2012

Keywords:
Flower-like
Composite
Microwave
Photocatalytic activity

ABSTRACT

Flower-like Bi_2WO_6 and Bi_2O_3–Bi_2WO_6 composite microstructures have been synthesized via a facile and rapid microwave-assisted hydrothermal method through controlling the experimental parameters. The phases and morphologies of the products are characterized by powder X-ray diffraction (XRD), energy dispersion X-ray analysis (EDX), high resolution transmission electron microscopy (HRTEM), and scanning electron microscopy (SEM). Photocatalytic experiments indicate that such Bi_2O_3–Bi_2WO_6 composite possesses higher photocatalytic activity for RhB degradation under visible-light irradiation in comparison with pure Bi_2O_3 and Bi_2WO_6. On the basis of the calculated energy band positions, the enhanced photocatalytic activity is attributed to the effective separation of electron–hole pairs between the two semiconductors. The present study provides a new strategy to design composite materials with enhanced photocatalytic activity.

1. Introduction

The effectiveness of solar-driven photocatalytic process underlying water splitting to supply clean and recyclable hydrogen energy and the degradation of organic pollutants is dictated to a great extent by the semiconductor's capability of absorbing visible and infrared light, as well as its ability to suppress the rapid combination of photogenerated electrons and holes [1–5]. However, how to improve the photocatalytic efficiency is still a great challenge to meet the requirements of future environmental and energy demands driven by solar energy. In recent years, the heterostructural composite of two semiconductors has been recognized as a promising method to develop a high efficiency photocatalytic material. Compared to a single semiconductor, heterostructures can promote efficient electron–hole separation and thus improve the photoelectrochemical activity [6–11]. For example, Kong et al. have synthesized the BiOBr–$ZnFe_2O_4$ heterostructures which were found to exhibit higher photocatalytic activity in visible-light degradation of rhodamine B than bare BiOBr and $ZnFe_2O_4$ [7].

Bismuth tungstate (Bi_2WO_6, n-type, band gap = 2.8 eV) is a promising visible-light-driven photocatalytic material and has recently stimulated intensive interest [10,12,13]. However, the rapid recombination of photoinduced electron–hole pairs seriously limits the energy-conversion efficiency. To improve the photocatalytic activity of Bi_2WO_6, many efforts in the fabrication of Bi_2WO_6-containing composites have been made. For example, Wang et al. [10] designed a Bi_2S_3/Bi_2WO_6 composite, which exhibited significantly enhanced photocatalytic activity for phenol degradation under visible-light irradiation. Bi_2O_3 is a p-type semiconductor with a band gap of ~2.8 eV and has proved to be a photocatalyst for water splitting and pollutant decomposing under visible-light irradiation [12,14–16]. Up to now, there have been few reports on Bi_2O_3–Bi_2WO_6 composite [12,16–18]. Chen et al. [12] have prepared Bi_2O_3–Bi_2WO_6 composite microspheres with enhanced photocatalytic performance through a one-step hydrothermal route with the aid of surfactant templates. Li et al. [16] synthesized Bi_2O_3–Bi_2WO_6 hollow microspheres via a hydrothermal method using polystyrene particles as the template. Zhang et al. [18] synthesized Bi_2O_3–Bi_2WO_6 photocatalysts by a solvothermal process using preformed Bi_2WO_6 as the substrate. These composite all exhibit higher photocatalytic activity than the single phased Bi_2WO_6 or Bi_2O_3. Microwave-assisted route has proved to be a very useful route to prepare various nanomaterials [19,20]. In this article, we describe a facile and rapid microwave-assisted hydrothermal approach to synthesize flower-like Bi_2WO_6 and Bi_2O_3–Bi_2WO_6 composite by adjusting the reaction conditions without the use of any surfactant or template. Furthermore, the experimental results confirm that these Bi_2O_3–Bi_2WO_6 composites exhibit much higher photocatalytic activities for degradation of RhB compared to pure Bi_2WO_6 and Bi_2O_3.

* Corresponding author. Fax: +86 25 83314502.
E-mail address: xtchen@netra.nju.edu.cn (X.-T. Chen).

0021-9797/$ - see front matter © 2012 Elsevier Inc. All rights reserved.
http://dx.doi.org/10.1016/j.jcis.2012.12.002

2. Experimental section

2.1. Synthesis of flower-like Bi_2WO_6 and Bi_2O_3–Bi_2WO_6 microstructures

All of the reagents were of analytical grade and were used without any further purification. In a typical procedure, a mixture of $Bi(NO_3)_3{\cdot}5H_2O$ (1.0 mmol) and $Na_2WO_4{\cdot}2H_2O$ (2.0 mmol) in 15 mL of distilled water was stirred for 30 min, followed by addition of 2 ml of ethylenediamine (En, 99%). After being stirred for 30 min, the mixture was transferred into a 35 mL round-bottom flask in a microwave system (2.45 GHz, Discover S-Class, CEM) equipped with *in situ* magnetic stirring. After treating the mixture at 180 °C for 10 min under microwave radiation, the resulting product was cooled to room temperature rapidly by air compressor. The product (the typical sample, named as T180) was collected, washed with deionized water and absolute ethanol for several times, and dried in vacuum at 80 °C for 12 h. Other experiments were also conducted under different conditions by using similar procedures. For the convenience of description, the products synthesized under different conditions were denoted as in Table 1. Besides, the series of samples prepared at different time (140–180 °C), with different amount of $Na_2WO_4{\cdot}2H_2O$ (0–1.5 mmol), for different reaction time (1–8 min) and with different amount of ethylenediamine (0–1 ml) are labeled T, W, t, and E, respectively. For example, T140, T150, T160, T170, and T180 represent the samples prepared at 140, 150, 160, 170, and 180 °C, while the other reaction conditions were kept constant, see Table 1.

2.2. Materials characterization

The phases of the products were characterized by X-ray powder diffraction (XRD) with a Shimadzu XRD-6000 powder X-ray diffractometer with Cu Kα radiation (λ = 1.5418 Å), recorded with 2θ ranging from 10° to 70°. Selected area electron diffraction (SEAD) and transmission electron microscopy (TEM) were carried out on a JEM-2100 high resolution transmission microscope, employing an accelerating voltage of 200 kV. Scanning electron microscopy (SEM) images and energy dispersion X-ray analysis (EDX) of the products were obtained on a field emission scanning electron microanalyser (Hitachi S-4800), employing an accelerating voltage of 10 kV or 20 kV by depositing the products on a conductive adhesive tape. X-ray photoelectron spectroscopy (XPS) was recorded on a PHI 5000 VersaProbe X-ray photoelectron spectrometer, using Al Kα monochromatic X-ray radiation (1486.6 eV). The peak positions were calibrated against the reference C 1s peak (284.8 eV) of contaminated carbon. The UV–vis diffusion reflectance spectra (DRS) of the samples were analyzed with a UV–vis spectrophotometer (UV-3600, Shimadzu, Japan) and $BaSO_4$ was used as reference. X-ray fluorescence (XRF) of the samples was analyzed with Shimadzu EDX-720/800HS/900HS.

2.3. Photodegradation experiments

The photocatalytic degradation of rhodamine B (RhB) or phenol was conducted in an XPA-photochemical reactor (Xujiang Electromechanical Plant, Nanjing, China) equipped with a 400 W metal halide lamp and a cutoff filter ($\lambda \geqslant 420$ nm). An electric fan and cooling water were used to eliminate thermal effect. The photocatalyst (0.02 g) was introduced into a Pyrex reactor containing 20 ml of RhB (10^{-5} mol/L) or phenol (40 mg/L) aqueous solution at room temperature in the air. Before light was turned on, the solution was continuously stirred for 30 min in the dark to ensure the establishment of an adsorption–desorption equilibrium. Then the photocatalytic reaction was initiated. At given time intervals, a portion of the suspension was removed from the reactor, centrifuged, and filtered to remove the catalyst particles before analysis. The RhB or phenol concentration was analyzed through a UV–vis spectrophotometer (Shimadzu, UV-3600). In order to determine the durability of the photocatalyst, the photocatalyst was separated from aqueous solution after each run. The filtered solid was reused in the subsequent recycling experiment without any treatment.

3. Results and discussion

3.1. Structure and morphology characterization

The crystalline structure of the products (samples T180 and W0.5) was investigated by the powder X-ray diffraction (XRD). Fig. 1a indicates that all the peaks of T180, which was prepared at 180 °C with 2 mmol of $Na_2WO_4{\cdot}2H_2O$ for 10 min, are readily indexed to the russellite Bi_2WO_6 with pure phase (JCPDS file Card No. 73-1126). The diffraction profile of Fig. 1b shows that sample W0.5, which was prepared at 180 °C with 0.5 mmol of $Na_2WO_4{\cdot}2H_2O$ for 10 min, was composed of russellite Bi_2WO_6 (JCPDS file Card No. 73-1126) and cubic Bi_2O_3 (JCPDS file Card No. 74-1373). No other phases can be found in these patterns. The chemical composition of T180 was further analyzed using energy dispersive X-ray

Table 1
The detailed reaction conditions and the final morphologies for the samples.

Sample[a]	Reaction conditions					Final morphology
	Bi Source (mmol)	W Source (mmol)	En (ml)	Temperature (°C)	Time (min)	
T180	1	2	2	180	10	Flower-like Bi_2WO_6 microstructures
T170	1	2	2	170	10	Flower-like Bi_2WO_6 microstructures
T160	1	2	2	160	10	Bi_2O_3 nanoparticles + flower-like Bi_2WO_6 microstructures
T150	1	2	2	150	10	Bi_2O_3 nanoparticles + flower-like Bi_2WO_6 microstructures
T140	1	2	2	140	10	Bi_2O_3 nanoparticles
W1.5	1	1.5	2	180	10	Flower-like Bi_2WO_6 microstructures
W1	1	1	2	180	10	Flower-like Bi_2WO_6 microstructures
W0.5	1	0.5	2	180	10	Bi_2O_3 nanoparticles + flower-like Bi_2WO_6 microstructures
W0	1	0	2	180	10	Nanosheets (unable to be identified)
t1	1	2	2	180	1	Bi_2O_3 nanoparticles
t2	1	2	2	180	2	Bi_2O_3 nanoparticles + flower-like Bi_2WO_6 microstructures
t5	1	2	2	180	5	Bi_2O_3 nanoparticles + flower-like Bi_2WO_6 microstructures
t8	1	2	2	180	8	Bi_2O_3 nanoparticles + flower-like Bi_2WO_6 microstructures
E1	1	2	1	180	10	Bi_2WO_6 nanoflakes
E0.5	1	2	0.5	180	10	Bi_2WO_6 nanoflakes
E0	1	2	0	180	10	Amorphous products

[a] The samples prepared with different reaction conditions were labeled T, W, t, and E.

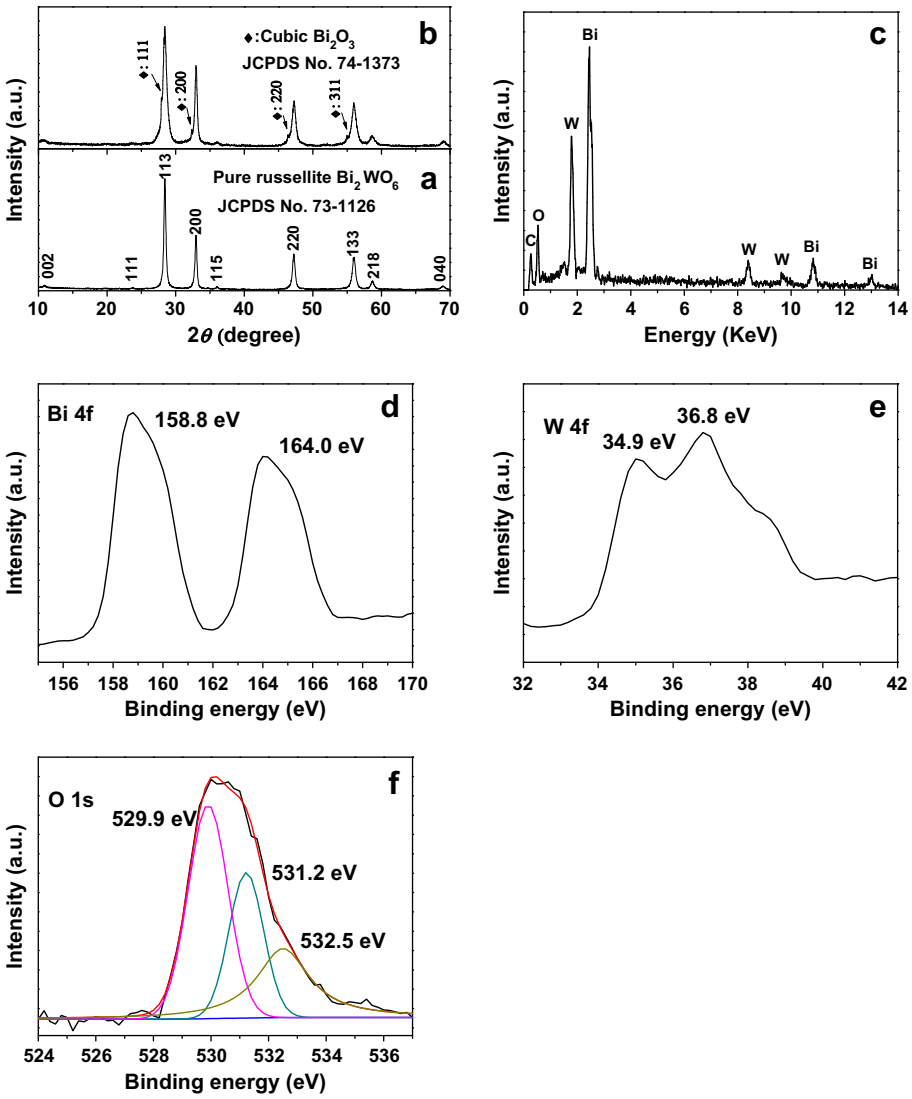

Fig. 1. (a) XRD and (c) EDX patterns of Bi_2WO_4 (T180) prepared at 180 °C with 2 mmol $Na_2WO_4{\cdot}2H_2O$ for 10 min. (b) XRD pattern and (d–f) XPS spectra of the Bi_2O_3–Bi_2WO_6 composite (W0.5) prepared at 180 °C with 0.5 mmol of $Na_2WO_4{\cdot}2H_2O$ for 10 min.

spectroscopy (EDX, Fig. 1c). The peaks of Bi, W and O can be easily found. The C peak in the spectrum could be attributed to the carbon on the conductive adhesive tape used to hold the sample.

The surface composition and state of the product (W0.5) were further investigated using X-ray photoelectron spectroscopy (XPS). As shown in Fig. 1d, the two peaks located at 164.0 and 158.8 eV can be attributed to Bi $4f_{5/2}$ and Bi $4f_{3/2}$ [18], respectively. The two peaks at the W region of 36.8 and 34.9 eV can be assigned to the binding energy of W 4f (Fig. 1e) [18]. Because of the existence of several types of nonequivalent lattice O atoms, the XPS spectrum in the O 1s region is complicated and can be deconvoluted to three peaks at 532.5, 529.9, and 531.2 eV (Fig. 1f), which can be assigned to Bi–O in Bi_2O_3 and Bi–O and W–O in Bi_2WO_6, respectively [16,18]. The results reveal the co-existence of Bi_2O_3 and Bi_2WO_6, which is in good agreement with the above XRD analysis.

The morphologies of the final products are characterized by SEM and TEM. Fig. 2a is a typical low-magnification SEM image of T180, which is composed of many uniform flower-like microstructures with a diameter of ca. 5 μm. The high-magnification SEM image (Fig. 2b) reveals that the flower-like microstructure is built from many thin sheets with a thickness about 10 nm. These nanoflakes are intercrossed each other and aggregated together to form flower-like microstructures. The SEM image of the as-obtained Bi_2O_3–Bi_2WO_6 composite (W0.5) was shown in Fig. 2c–e, showing that the sample consists of hierarchical structures with nanoparticles embedded in the sheets. The TEM image is in agreement with the SEM characterization (Fig. 2f). To further confirm the composition of the composite, the sample was characterized by HRTEM analysis. The lattice fringes with interplanar spacing of 0.41 nm on the HRTEM image (Fig. 2g), which is on the area marked g in Fig. 2f corresponds to the (004) plane of Bi_2WO_6, while the fringes of $d = 0.32$ nm in Fig. 2h observes on the area marked h in Fig. 2f matches the (111) planes of cubic Bi_2O_3. These analyses indicate that the Bi_2O_3–Bi_2WO_6 composite was obtained.

3.2. Factors influencing the formation of the flower-like Bi_2WO_6 and Bi_2O_3–Bi_2WO_6 heterostructures

In order to reveal the factors influencing the formation of flower-like Bi_2WO_6 and Bi_2O_3–Bi_2WO_6, a series of controlled experiments have been carefully performed whereby one reaction parameter (volume of ethylenediamine, amount of $Na_2WO_4{\cdot}2H_2O$,

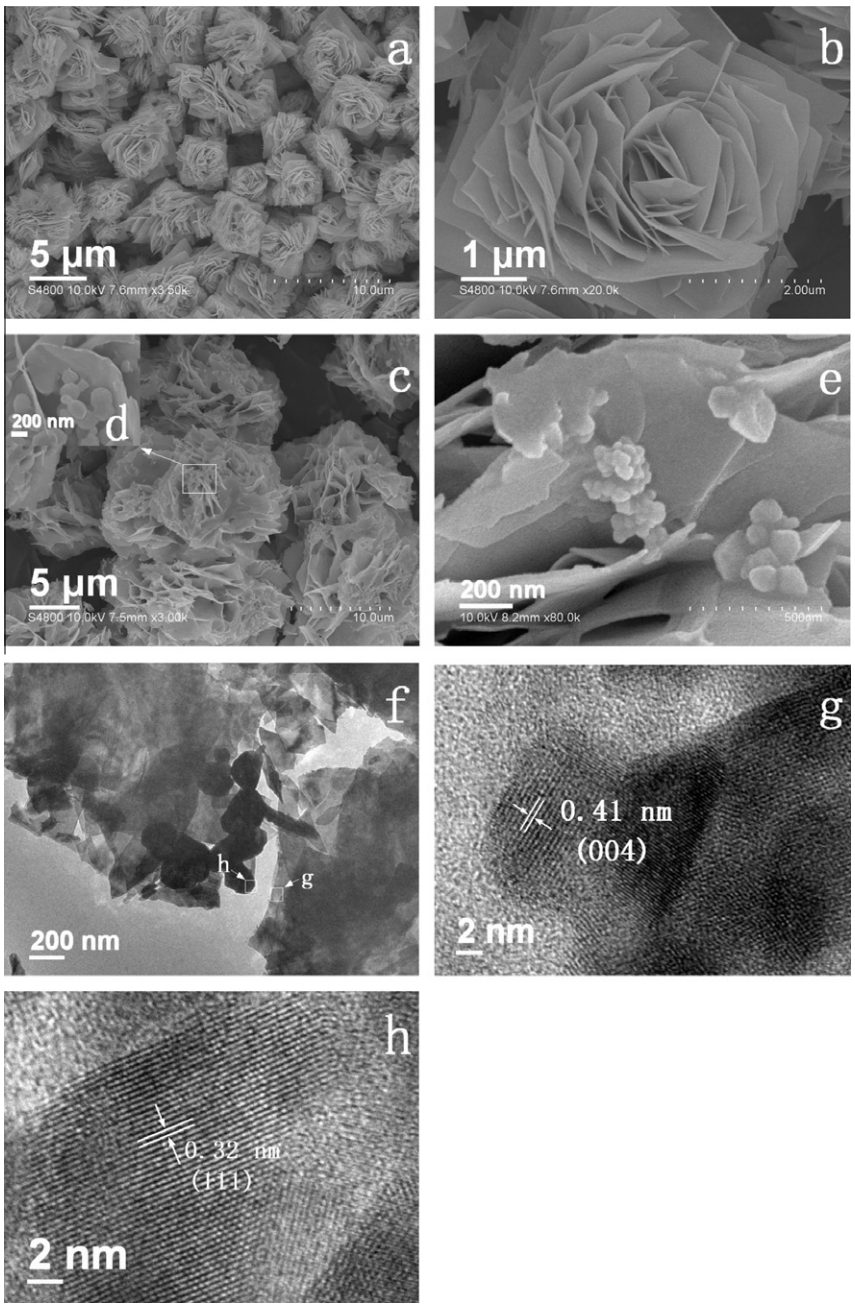

Fig. 2. (a and b) SEM images of Bi_2WO_4 (sample T180) prepared with 2 mmol of $Na_2WO_4{\cdot}2H_2O$ at 180 °C for 10 min. (c–e) SEM, (f) TEM and (g and h) HRTEM images of the Bi_2O_3–Bi_2WO_6 composite (sample W0.5) prepared with 0.5 mmol of $Na_2WO_4{\cdot}2H_2O$ at 180 °C for 10 min.

reaction time, and temperature) was changed while the other reaction conditions were kept constant.

3.3. Effect of the reaction temperature

The reaction temperature is known to be an important parameter affecting greatly the morphology of the samples prepared in hydrothermal processes. Controlled experiments have been carried out at different reaction times to yield samples T140-T180 (Table 1). When the temperature was controlled at 140 °C, the product (T140) was composed of many Bi_2O_3 nanoparticles with different sizes (Fig. 3a and e). Increasing the temperature to 150 °C, the product (T150) contains a mixture of flower-like microstructures and nanoparticles (Fig. 3b). The corresponding XRD pattern shown in Fig. 3e indicates that T150 is a mixture of Bi_2WO_6 (JCPDS file Card No. 73-11126) and Bi_2O_3 (JCPDS file Card No. 74-1373). Further increasing the temperature to 160 °C, the bulk of the product (T160) is Bi_2WO_6 flower-like microstructures, accompanied by some Bi_2O_3 nanoparticles adhered on the nanosheets (Fig. 3c and e). When the reaction temperature was controlled at 170 °C, the nanoparticles vanished and only pure flower-like Bi_2WO_6 microstructures were obtained (Fig. 3d and e). At 180 °C, the novel Bi_2WO_6 flower-like microstructures were harvested (Fig. 2a). The products obtained at 170 and 180 °C were indexed to Bi_2WO_6 (JCPDS file Card No. 73-11126) (Figs. 1a and 3e). These experimental results indicate that the increase in the reaction temperature will facilitate the transformation from Bi_2O_3 to Bi_2WO_6. At lower temperature, Bi_2O_3 was easily obtained. There have been some reports of preparation of Bi_2O_3 at low temperature. For example, Li et al. [21] synthesized Bi_2O_3 nanostructures by a citrate-assisted

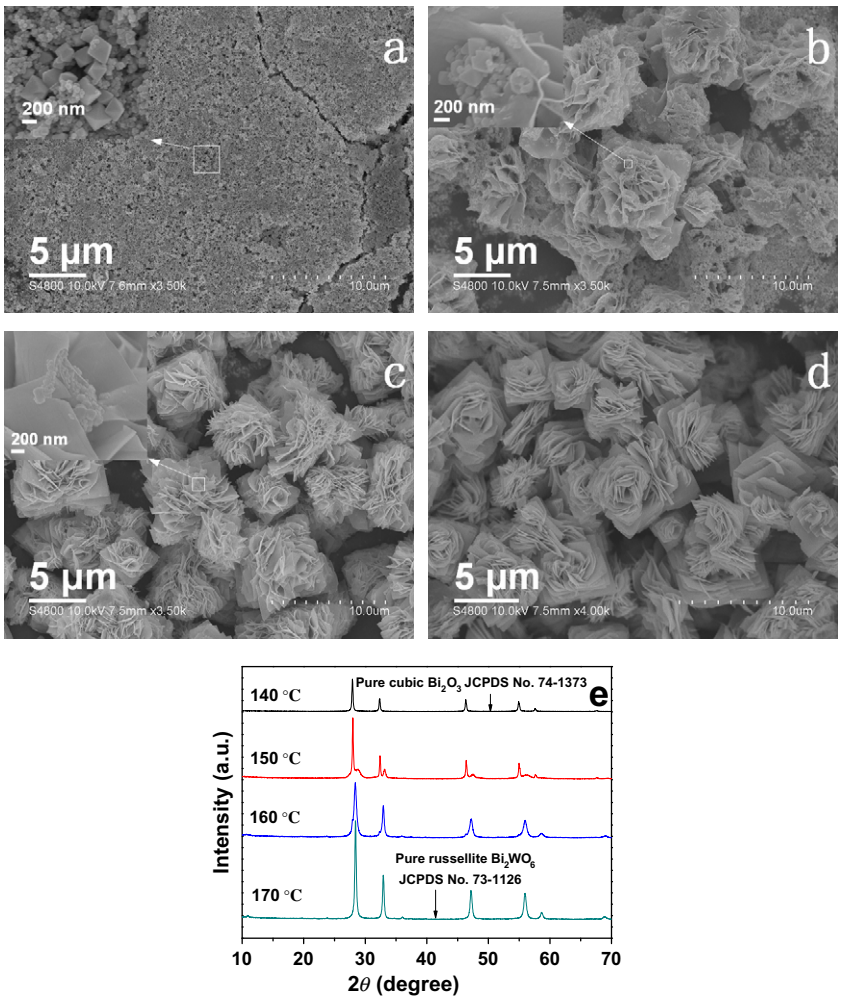

Fig. 3. SEM images of products from reactions for 10 min at different temperatures: (a) 140 °C, (b) 150 °C, (c) 160 °C and (d) 170 °C; and (e) their XRD patterns (T140, T150, T160 and T170).

solution approach at 40 °C. Wang and co-workers [15] prepared Bi_2O_3 hierarchical nanostructures at 60–80 °C.

3.3.1. Effect of ethylenediamine

In recent years, many reports suggest that the alkylamine could mediate the crystal structure evolution and control the complex morphology because they absorb on solid surfaces and selectively bind to some specific crystalline planes to control the direction of crystal growth [22–24]. In this work, ethylenediamine was used to synthesize flower-like Bi_2WO_6 microstructures. The effect of the amount of ethylenediamine has been studied (see E0, E0.5 and E1 in Table 1). Without the addition of ethylenediamine, the morphology is irregular and the product (E0) is amorphous phase (Fig. 4a and d). When 0.5 or 1 ml of ethylenediamine was added, the products (E0.5, E1) were all Bi_2WO_6 nanoflakes (Fig. 4b and c). Further increasing the volume of ethylenediamine to 2 ml, novel flower-like microstructures were the final product (Fig. 2a). The phases of the three products were all pure russellite Bi_2WO_6 (Figs. 1a and 4d). These observations suggest that ethylenediamine played a key role in the formation of hierarchical microstructures. In this study, suitable volume of ethylenediamine is important for the morphology control of the sample.

3.3.2. Effect of the amount of $Na_2WO_4{\cdot}2H_2O$

It was found that the amount of $Na_2WO_4{\cdot}2H_2O$ had a marked influence on the morphologies of the final products (see W0–W1.5 in Table 1). In the absence of $Na_2WO_4{\cdot}2H_2O$, nanosheets were the final product (W0, Fig. 5a), but the XRD pattern of the product could not be identified in the standard JCPDS cards (Fig. 5d). When 0.5 mmol of $Na_2WO_4{\cdot}2H_2O$ was added, Bi_2O_3–Bi_2WO_6 composites (W0.5) were obtained (Figs. 1b and 2c). When 1 or 1.5 mmol of $Na_2WO_4{\cdot}2H_2O$ was employed, incomplete flower-like microstructures were produced (W1, W1.5, Fig. 5b and c). Further increasing the amount to 2 mmol, the novel flower-like microstructures were obtained (Fig. 2a). When the amount was controlled at 1, 1.5 or 2 mmol, the phases of the products could be indexed to pure russellite Bi_2WO_6 (Figs. 1a and 5d). These observations indicate that the formation of flower-like Bi_2WO_6 microstructures depends on the amount of the reactant $Na_2WO_4{\cdot}2H_2O$.

3.3.3. Time-dependent experiments and the mechanism of formation

Time-dependent experiments were carried out to understand the formation process of flower-like microstructures and heterostructures (t1–t8 and T180 in Table 1). Fig. 6 shows the SEM images of the samples obtained with different reaction times. At the early stage of the reaction (1 min), the product (t1) is composed of irregular and octahedral nanoparticles (Fig. 6a), and the phase was confirmed as pure cubic Bi_2O_3 by XRD (Fig. 6e). Although the cubic phase Bi_2O_3 (δ-Bi_2O_3) is a high-temperature phase which usually exists at >730 °C, dopants such as rare-earth elements and many oxide impurities may stabilize it [25]. For example, Wang et al. [15] synthesized δ-Bi_2O_3 by introducing

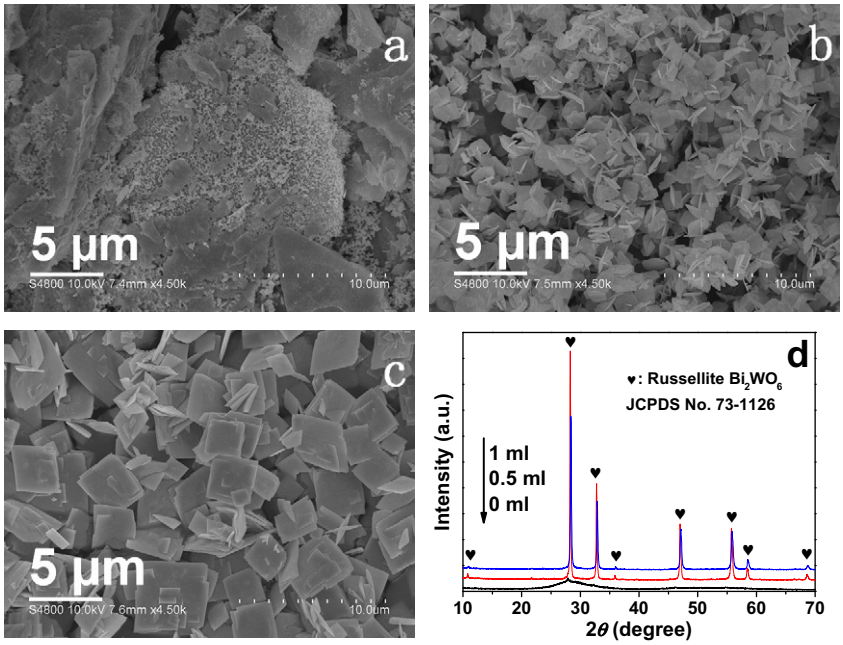

Fig. 4. SEM images of the as-prepared products at 180 °C for 10 min with different volume of ethylenediamine: (a) 0 ml, (b) 0.5 ml and (c) 1 ml; and (d) their XRD patterns (E0, E0.5 and E1).

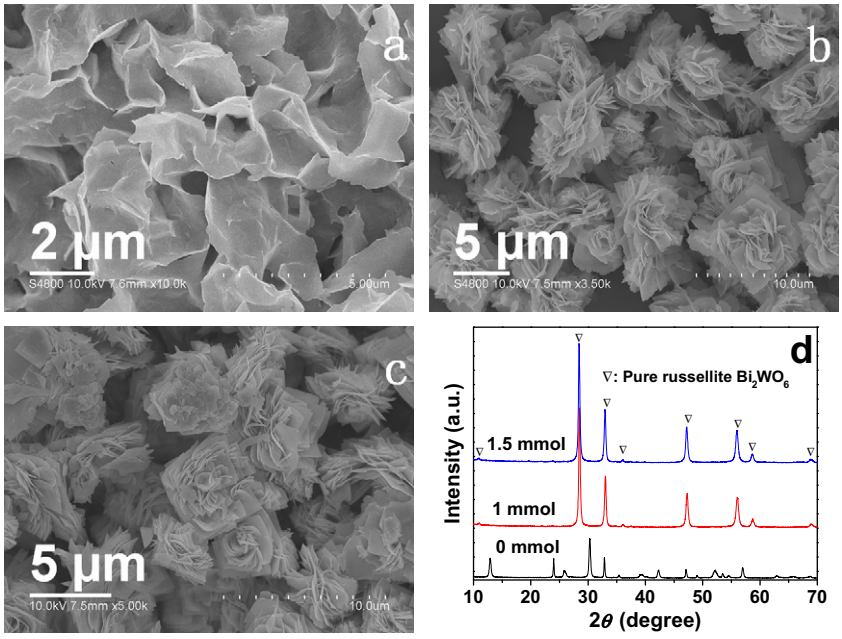

Fig. 5. SEM images of the as-prepared products at 180 °C for 10 min with different amount of $Na_2WO_4{\cdot}2H_2O$: (a) 0 mmol, (b) 1 mmol, (c) 1.5 mmol; and (d) their XRD patterns (W0, W1 and W1.5).

VO_3^- into the reaction system at 60–80 °C. In this work, the δ-Bi_2O_3 phase formed at the early stage of the reaction was confirmed to be doped with W by an EDX analysis (Fig. 6f). Increasing the reaction time to 2 min, some complex microstructures could be found (T2, Fig. 6b). When the reaction time was increased to 5 and 8 min, the complex microstructures (T5, T8) were the dominant product and the number of nanoparticles decreased (Fig. 6c and d). All phases of the products obtained at 2, 5, and 8 min were mixtures of cubic Bi_2O_3 and russellite Bi_2WO_6 (Fig. 1a and 6e), indicating that Bi_2O_3–Bi_2WO_6 heterostructures could be obtained by controlling the reaction time. For a reaction time of 10 min, well-defined flower-like microstructures were formed without nanoparticles. The results here indicate that by increasing the reaction time, the Bi_2O_3 nanoparticles gradually disappear, forming more and more flower-like Bi_2WO_6 microstructures.

A mechanism of the formation and the conversion of cubic Bi_2O_3 to russellite Bi_2WO_6 flower-like microstructures is proposed below. In the reaction, microwave might favor the fast formation of Bi_2O_3 and growth of Bi_2WO_6 flower-like microstructures. The formation mechanism could be explained by the Ostwald ripening process, as the results in the current work are consistent with previous reports on Ostwald ripening [15,26–28]. In the early stage,

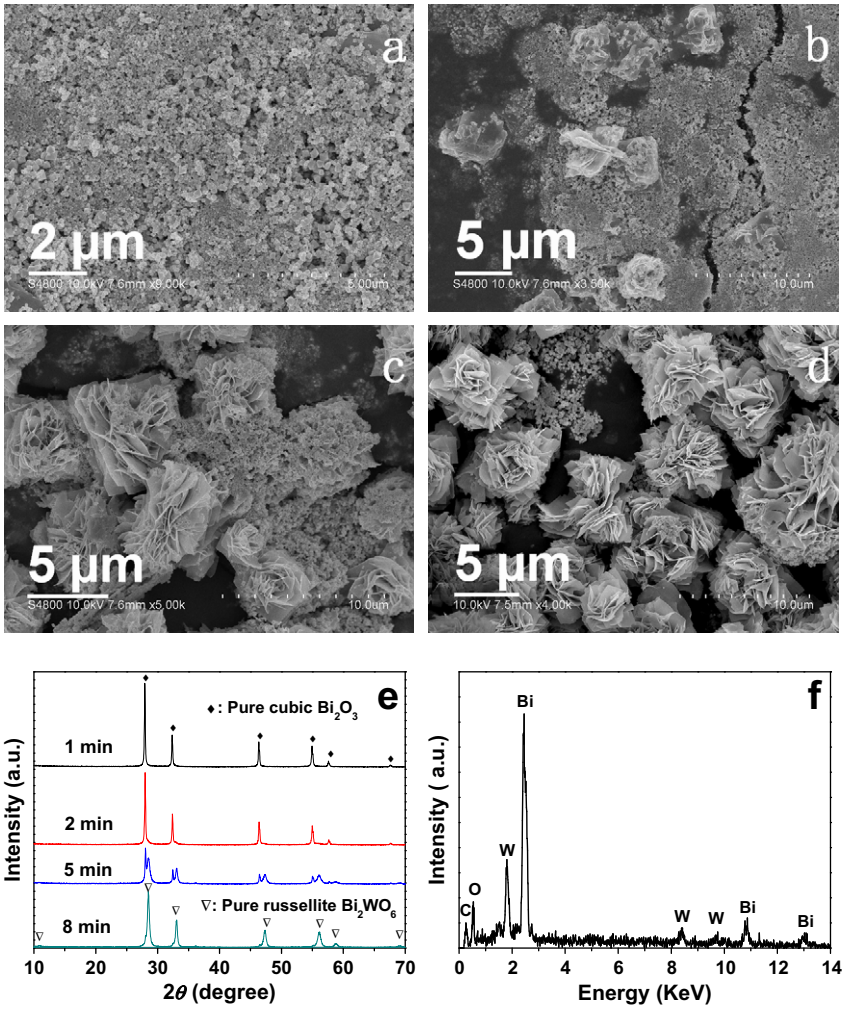

Fig. 6. SEM images of the as-prepared products at 180 °C for different reaction time: (a) 1 min, (b) 2 min, (c) 5 min and (d) 8 min; and (e) their XRD patterns (t1, t2, t5 and t8). (f) EDX pattern of the product (t1) at 180 °C for 1 min.

Bi_2O_3 nanoparticles were easily obtained in the presence of base. At the constant reaction temperature of 180 °C, the nanoparticles started to dissolve into the solution and spontaneously nucleated into Bi_2WO_6 nanosheets with WO_4^{2-}. As the mass diffusion and Ostawald process proceeded, the nanosheets grew until all the nanoparticles were consumed, accompanied by self-assembly of these nanosheets into hierarchical microstructures. Ethylenediamine may affect the conversion of intercrossed nanosheets to the hierarchical microstructures. Recently, our group [29] has reported the synthesis of hierarchical Bi_2MoO_6 microstructures in the presence of ethylenediamine. We investigated the effect of ethylenediamine on the formation of hierarchical Bi_2MoO_6 microstructures and found that ethylenediamine can really facilitate the formation of hierarchical structures. In this study, ethylenediamine may play the similar effect. As the time proceeded, the Bi_2O_3 nanoparticles vanished and the flower-like microstructures formed.

3.4. Optical properties and photocatalytic performances

The room temperature UV–vis absorption spectra of pure Bi_2O_3 (t1), Bi_2WO_6 (T180), and Bi_2O_3–Bi_2WO_6 composite (t8, W0.5 and T160) are shown in Fig. 7. The band gaps (E_g) of pure Bi_2O_3 and Bi_2WO_6 are estimated to be ca. 2.77 and 2.75 eV, respectively. Here, E_g was derived from $E_g = 1239.8/\lambda_g$, where λ_g is the absorption edge in the UV–vis spectra [7]. Because the band gaps of pure Bi_2O_3 and Bi_2WO_6 are similar, the absorption edges of Bi_2O_3–Bi_2WO_6 composites (T160, W0.5, and t8) showed no obvious change, but the absorption intensities were increased.

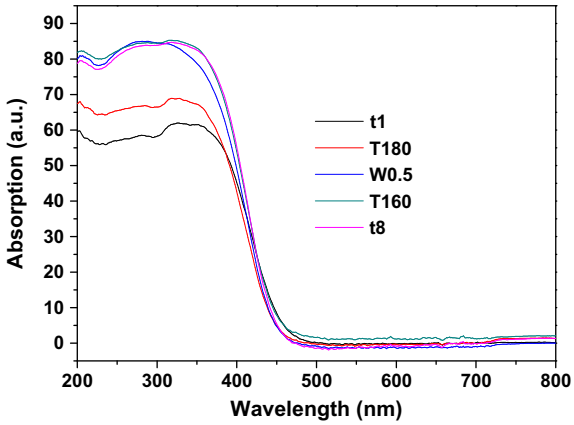

Fig. 7. Ultraviolet–visible diffusive absorption spectra of the as-obtained samples.

The visible-light-driven photocatalytic activities of the as-synthesized samples were measured by monitoring the change in optical absorption of the RhB solution at ~554 nm during its photocatalytic decomposition process. As shown in Fig. 8A, all the

photocatalysts showed photocatalytic activities under visible-light irradiation. More importantly, RhB itself was not decomposed in the absence of the catalyst. Pure Bi_2O_3 (t1) showed weak activity less than 8% RhB was decomposed after 100 min of irradiation. It should be noted that all the Bi_2O_3–Bi_2WO_6 samples (T160, t8, and W0.5) showed higher activity than pure Bi_2WO_6 sample (T180) and the highest activity was observed for sample W0.5, with which about 95% RhB was degraded in 60 min of visible-light irradiation.

The molar percentage of Bi_2O_3 and Bi_2WO_6 may have a great effect on the photocatalytic activity of Bi_2O_3–Bi_2WO_6 composite; therefore, we analyzed the quantitative chemical composition of the three Bi_2O_3–Bi_2WO_6 composites by X-ray fluorescence spectroscopy (XRF). The results demonstrate that the molar ratio of Bi/W is 2.19:1 (t8), 2.35:1 (T160), 2.38:1 (W0.5), namely, the fractions of Bi_2O_3 in the three nanocomposites are 8.7%, 14.9%, 16% for t8, T160, and W0.5, respectively. It appears that the more percentage of Bi_2O_3 corresponds to the higher photocatalytic activity (W0.5). It is possible that appropriate content of Bi_2O_3 is crucial for high performance photocatalytic activity of the Bi_2O_3–Bi_2WO_6 composite. Zhang et al. [18] have studied the effect of loading amount of Bi_2O_3 on the photocatalytic performance of the Bi_2O_3/Bi_2WO_6 catalyst. They found that the optimum content for the highest catalytic activity is 3 wt.% Bi_2O_3 in their obtained Bi_2O_3/Bi_2WO_6 photocatalyst. In this study, less amount of Bi_2O_3 may also reduce the photocatalytic property of the Bi_2O_3–Bi_2WO_6 composite.

The results of cycling tests demonstrating the visible-light-driven photocatalytic activity of sample W0.5 in decomposing RhB are shown in Fig. 8B. Only a little reduction of its photocatalytic activity after six photocatalysis cycles was observed, which might be due to the loss of catalysts during cycling tests.

To exclude the photosensitization effect, the typical colorless contaminant phenol was also used as the model pollutant instead of RhB to test the photocatalytic activity of sample W0.5. As shown in Fig. 8C, blank tests (phenol solution without any photocatalyst) under visible light exhibit little photodegradation, indicating that phenol is stable under visible light. Under identical experimental conditions, 40% of phenol could be photodegradated after 12 h visible-light irradiation in the presence of the as-obtained Bi_2O_3–Bi_2WO_6 composite (W0.5). Therefore, the result indicates that the photocatalytic property of Bi_2O_3–Bi_2WO_6 composite is not induced by photosensitization effect.

3.5. Photocatalytic mechanism

To understand the mechanism of the enhanced photocatalytic activity of the Bi_2O_3–Bi_2WO_6 composite, the potentials of conductance and valence band (CB and VB) edges of Bi_2O_3 and Bi_2WO_6 were investigated using the equation related to the Mulliken electronegativity and the band gap of a semiconductor,

$$E_{CB} = X - E_e - 0.5E_g,$$

where E_{CB} and E_g are the bottom position of CB relative to the *NHE* level and band gap of the semiconductor, respectively, and X is the geometric mean of the Mulliken electronegativities of the constituent atoms in the semiconductor, and E_e is the energy of free electrons on the hydrogen scale (~4.5 eV) [30,31]. The X values for Bi_2WO_6 and Bi_2O_3 are calculated to be 6.33 and 6.12, and both of the band gap energies of Bi_2WO_6 and Bi_2O_3 are ~2.8 eV [10,12,18]. E_{CB} of Bi_2WO_6 and Bi_2O_3 is determined to be 0.46 and 0.22 eV relative to the *NHE* level, respectively. Correspondingly, the E_{VB} of Bi_2WO_6 and Bi_2O_3 is obtained to be 3.26 and 3.02 eV, respectively. These band potentials imply that p–n heterojunction could form in the interface between Bi_2WO_6 and Bi_2O_3, which is responsible for the enhanced photocatalyitc activity of Bi_2O_3–Bi_2WO_6 composite. The plausible photocatalytic mechanism is shown in Fig. 9. In the Bi_2O_3–Bi_2WO_6 composite, both the Bi_2O_3 and Bi_2WO_6 are excited by visible light. When photons are

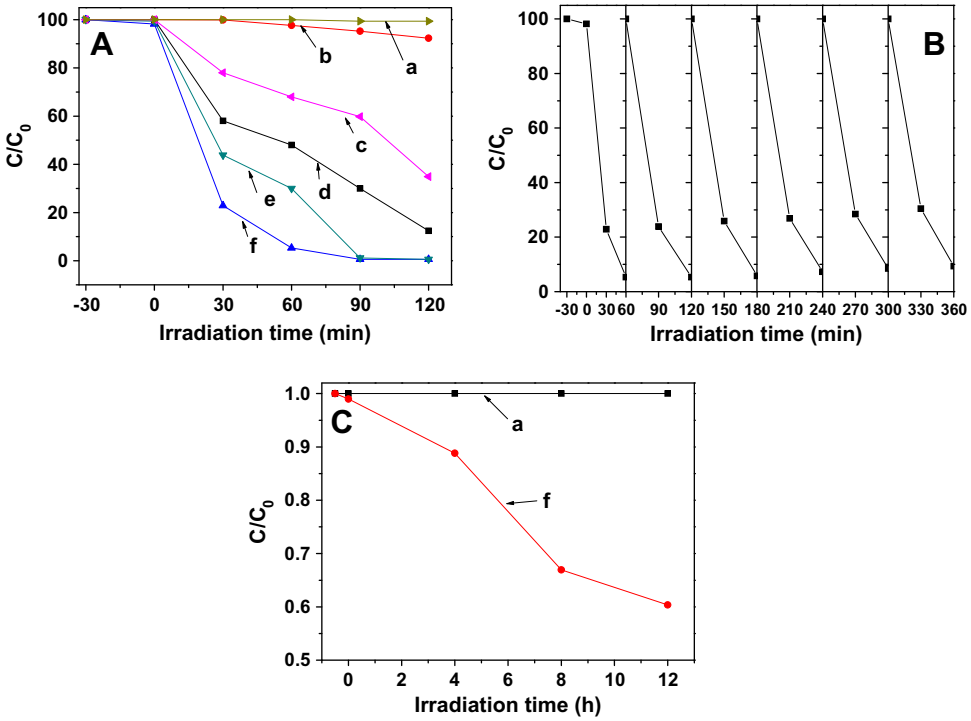

Fig. 8. (A) Comparison of the visible-light (⩾420 nm)-driven photocatalytic activity under the same experimental conditions: (a) without photocatalyst, (b) pure Bi_2O_3 (t1), (c) pure Bi_2WO_6 (T180), (d) t8, (e) T160, (f) W0.5. (B) Cycling tests of visible-light-driven photocatalytic activity (RhB decomposition) of sample W0.5. (C) Variation of phenol concentration as a function of irradiation time under visible-light (⩾420 nm): (a) without photocatalyst and (f) W0.5.

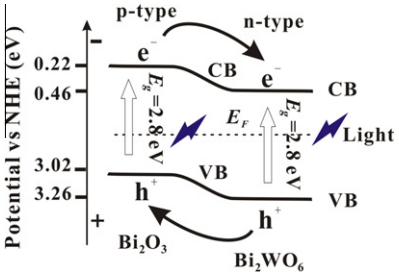

Fig. 9. Schematics of the potential energy diagram for the Bi_2O_3–Bi_2WO_6 p–n heterostructural composite.

absorbed by the composite, electron–hole pairs are generated. Holes then move to the p-type Bi_2O_3 side and electron to the n-type Bi_2WO_6 side. The resulting separation of photogenerated electrons and holes may facilitate the transfer of charge carriers and retard the e^-–h^+ recombination, thus resulting in improved photocatalytic performance [7,8,16,18].

4. Conclusions

In summary, flower-like Bi_2WO_6 microstructures have been synthesized via a facile and rapid microwave-assisted hydrothermal method. Several factors influencing the formation of the flower-like Bi_2WO_6 microstructures have been studied. By adjusting the experimental conditions, the Bi_2O_3–Bi_2WO_6 composite was obtained. Such Bi_2O_3–Bi_2WO_6 composite has been demonstrated to higher photocatalytic activities than pure Bi_2O_3 and Bi_2WO_6. The enhanced activity is attributed to the effective separation of electron–holes pairs as a result of the formation of p–n heterojunction between the two semiconductors.

Acknowledgments

This work was supported by the National Basic Research Program of China (No. 2013CB922102), Natural Science Grant of China (No. 21021062), and the US National Science Foundation (CHE-1012173).

References

[1] X.B. Chen, L. Liu, P.Y. Yu, S.S. Mao, Science 331 (2011) 746–750.
[2] S.U.M. Khan, M. Al-Shahry, W.B. Ingler, Science 297 (2002) 2243–2245.
[3] H. Tong, S.X. Ouyang, Y.P. Bi, N. Umezawa, M. Oshikiri, J.H. Ye, Adv. Mater. 24 (2012) 229–251.
[4] H.F. Cheng, B.B. Huang, Z.Y. Wang, X.Y. Qin, X.Y. Zhang, Y. Dai, Chem. Eur. J. 17 (2011) 8039–8043.
[5] A. Kubacka, M. Fernández-García, G. Colón, Chem. Rev. (2011) 1555–1614.
[6] H.G. Kim, P.H. Borse, J.S. Jang, E.D. Jeong, O.S. Jung, Y.J. Suh, J.S. Lee, Chem. Commun. (2009) 5889–5891.
[7] L. Kong, Z. Jiang, T.C. Xiao, L.F. Lu, M.O. Jones, P.P. Edwards, Chem. Commun. 47 (2011) 5512–5514.
[8] J.Z. Su, L.J. Guo, N.Z. Bao, C.A. Grimes, Nano Lett. 11 (2011) 1928–1933.
[9] J. Ren, W.Z. Wang, M. Shang, S.M. Sun, E.P. Gao, ACS Appl. Mater. Interface 3 (2011) 2529–2533.
[10] Z.J. Zhang, W.Z. Wang, L. Wang, S.M. Sun, ACS Appl. Mater. Interface 4 (2012) 593–597.
[11] S.J. Hong, S. Lee, J.S. Jang, J.S. Lee, Energy Environ. Sci. 4 (2011) 1781–1787.
[12] M. Ge, Y.F. Li, L. Liu, Z. Zhou, W. Chen, J. Phys. Chem. C 115 (2011) 5220–5225.
[13] L.W. Zhang, Y.J. Wang, H.Y. Cheng, W.Q. Yao, Y.F. Zhu, Adv. Mater. 21 (2009) 1286–1290.
[14] Y. Wang, S.K. Li, X.R. Xing, F.Z. Huang, Y.H. Shen, A.J. Xie, X.F. Wang, J. Zhang, Chem. Eur. J. 17 (2011) 4802–4808.
[15] L. Zhou, W.Z. Wang, H.L. Xu, S.M. Sun, M. Shang, Chem. Eur. J. 15 (2009) 1776–1782.
[16] X.N. Li, R.K. Huang, Y.H. Hu, Y.J. Chen, W.J. Liu, R.S. Yuan, Z.H. Li, Inorg. Chem. 51 (2012) 6245–6250.
[17] M.S. Gui, W.D. Zhang, J. Phys. Chem. Solids 73 (2012) 1342–1349.
[18] M.S. Gui, W.D. Zhang, Q.X. Su, C.H. Chen, J. Solid State Chem. 184 (2011) 1977–1982.
[19] M. Baghbanzadeh, L. Carbone, P.D. Cozzoli, C.O. Kappe, Angew. Chem. Int. Ed. 50 (2011) 11312–11359.
[20] I. Bilecka, M. Niederberger, Nanoscale 2 (2010) 1358–1374.
[21] H.B. Lu, S.M. Wang, L. Zhao, B.H. Dong, Z.X. Xu, J.C. Li, RSC Adv. 2 (2012) 3374–3378.
[22] Q. Liu, Y. Zhou, Y. Ma, Z.G. Zou, RSC Adv. 2 (2012) 3247–3250.
[23] W.T. Yao, S.H. Yu, Adv. Funct. Mater. 18 (2008) 3357–3366.
[24] H.B. Yao, M.R. Gao, S.H. Yu, Nanoscale 2 (2010) 323–334.
[25] R. Punn, A.M. Feteira, D.C. Sinclair, C. Greaves, J. Am. Chem. Soc. 128 (2006) 15386–15387.
[26] B. Hu, L.H. Wu, S.J. Liu, H.B. Yao, H.Y. Shi, G.P. Li, S.H. Yu, Chem. Commun. 46 (2010) 2277–2279.
[27] J. Li, H.C. Zeng, J. Am. Chem. Soc. 129 (2007) 15839–15847.
[28] B. Liu, H.C. Zeng, Small 1 (2005) 566–571.
[29] Z.Q. Li, X.T. Chen, Z.L. Xue, CrystEngComm (2012), http://dx.doi.org/10.1039/C2CE26260F.
[30] T.P. Cao, Y.J. Li, C.H. Wang, Z.Y. Zhang, M.Y. Zhang, C.L. Shao, Y.C. Liu, J. Mater. Chem. 21 (2011) 6922–6927.
[31] H.F. Shi, Z.S. Li, J.H. Kou, J.H. Ye, Z.G. Zou, J. Phys. Chem. C 115 (2011) 145–151.